ACS EARTH AND SPACE CHEMISTRY

http://pubs.acs.org/journal/aesccq

Article

Effects of Fullerol and Graphene Oxide on the Phase Transformation of Two-Line Ferrihydrite

Lixia Yan, Runliang Zhu,* Jing Liu, Yixuan Yang, Jianxi Zhu, Hongjuan Sun, and Hongping He

Cite This: *ACS Earth Space Chem.* 2020, 4, 335−344

Read Online

ACCESS | Metrics & More | Article Recommendations | Supporting Information

ABSTRACT: Two-line ferrihydrite (Fh) is an omnipresent iron oxyhydroxide nanomineral with high surface reactivity and weak crystallinity, and its phase transformation in nature has drawn significant concerns. A number of studies have investigated the effects of coexisting natural substances (e.g., ions, organic molecules, and clay minerals) on the phase transformation processes of Fh. This work, for the first time, studied the effects of coexisting carbon nanomaterials (CNM) on the phase transformation of Fh, and CNM with different morphologies, that is, graphene oxide (GO) and fullerol (PHF), were applied. Characterization results from X-ray diffraction, transmission electron microscopy, and Mössbauer spectroscopy showed that the transformed products of Fh are mainly hematite (Hem) with a small amount of goethite (Gth) in the absence/presence of CNM; however, the transformation kinetics, morphologies, and Hem/Gth ratio of the transformed products are distinctly different in each system. In particular, GO decreased the transformation rate of Fh (compared with the Fh system), whereas PHF not only accelerated the transformation rate but also favored the formation of larger Hem particles and higher Hem/Gth ratios in the transformed products. We hypothesized that these results could be attributed to the different behaviors of CNM in affecting the aggregation of Fh as the transformation of Fh into Hem is a solid phase transformation process (via dehydration), which strongly relies on the aggregation of Fh particles. In this term, the samples of CNM−Fh mixtures before transformation were characterized. The results obtained from atomic force microscopy and sedimentation experiments showed that the large lamellar GO could act as a dispersing agent and inhibit the aggregation and contact of Fh particles while the nanogranular PHF functioned as a "bridge" and enhanced the aggregation of Fh particles. This study revealed that the coexisting nanoparticles (e.g., PHF and GO) could exert different influences on the transformation of Fh by influencing its aggregation and dispersion.

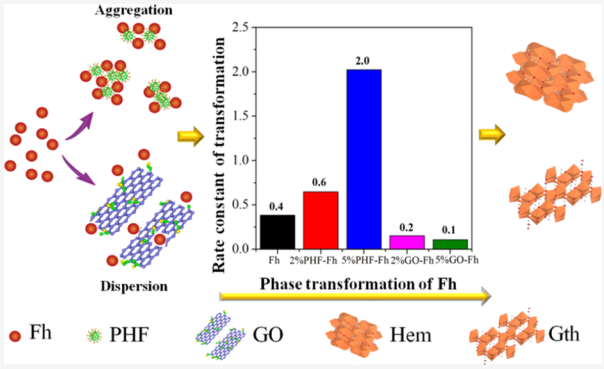

KEYWORDS: *ferrihydrite, nanomineral, transformation, carbon nanoparticles, aggregation, dispersion*

1. INTRODUCTION

Two-line ferrihydrite (hereafter denoted as Fh), a ubiquitous nanosized (2−4 nm) iron oxyhydroxide with large specific surface area and high surface reactivity, is an important sink for both metals and metalloids in the near-surface environment.[1−6] Fh is a poorly crystalline and thermodynamically unstable mineral with a short-range ordering structure[7,8] and can easily transform to other structurally stable iron (oxyhydr)oxide minerals, [e.g., to hematite (Hem) through aggregation and dehydration, and to goethite (Gth) through a dissolution and recrystallization mechanism].[1,9−11] As such, the components of iron (oxyhydr)oxides in the environment and the fate of the adsorbed chemicals (e.g., metals and metalloids) on the surface of Fh will be largely affected by the transformation pathways of Fh, which have been the subject of extensive study in the past decades.[12−14] Previous studies have shown that the transformation of Fh strongly depends on the environmental conditions (e.g., pH, Eh, temperature, and magnetic field).[9,15−17] For example, neutral pH conditions and high temperatures appear to favor the transformation of Fh to Hem, while acidic/alkaline pH and low temperatures always lead to the transformation of Fh to Gth.[15−17]

The effects of coexisting substances (e.g., ions, organic compounds, and mineral particles) on the transformation of Fh have also been well-studied, and the obtained results showed that coexisting substances may have quite different interactions with Fh particles, which accordingly may alter the transformation process of Fh.[1,9,18−20] For example, inorganic cations, oxyanions, neutral small molecules, and natural

Received: October 7, 2019
Revised: January 2, 2020
Accepted: February 25, 2020
Published: February 25, 2020

https://dx.doi.org/10.1021/acsearthspacechem.9b00261
ACS Earth Space Chem. 2020, 4, 335−344

polymers can be adsorbed onto the surface of Fh and generally will slow down its phase transformation rate by inhibiting the direct contact of Fh particles and/or reducing its dissolution.[20−24] Lamellar-structured clay minerals (e.g., montmorillonite) may separate Fh particles by functioning as "barriers" or release ions (e.g., Si and Al) under acidic/alkaline pH conditions to decrease the dissolution of Fh; in both cases, the phase transformation rate will be reduced as well.[19] Therefore, coexisting substances generally can inhibit the direct contact and/or reduce the dissolution of Fh particles, slowing down the transformation rate.[1] On the other hand, some other coexisting substances (e.g., Fe^{2+}, cysteine) that can transfer electrons to Fh may accelerate the transformation of Fh into Gth by enhancing its dissolution−recrystallization process.[25−27] Interestingly, most of the tested coexisting substances in previous studies are either small dissolved chemicals (e.g., ions and molecules) or a large solid phase (e.g., clay mineral particles), both of which do not have comparable size with Fh nanoparticles. One would, therefore, wonder whether some coexisting nanosized substances with different morphologies and particle sizes may have different effects on the phase transformation of Fh.

In fact, nanoparticles are ubiquitous in nature.[28−30] Among these nanoparticles, carbon nanomaterials (CNM) are important components, which can be both naturally and artificially produced from the widely distributed carbon-based compounds and materials.[31−35] The production of engineered CNM (e.g., carbon nanotube, fullerene, and graphene) is continuously increasing because of their wide industrial applications;[36,37] some natural processes (e.g., wildfire) can also produce large amounts of nanosized- or microsized carbon materials (e.g., biochar, charcoal, and soot).[38−40] In the near-surface environment, CNM will eventually be oxidized by photo-oxidation and natural oxidants.[41] These oxidized CNM [e.g., graphene oxide (GO) and fullerol (PHF)] generally have better hydrophilicity and higher mobility in natural environments;[41,42] thus, they have high chances to coexist and interact with the widespread Fh, affecting its phase transformation process. Indeed, several previous studies found that these oxidized CNM with different morphologies showed different interaction behaviors with Fe (oxyhydr)oxide.[42−45] For instance, Liu et al.[42] demonstrated that PHF can evidently enhance the aggregation of Fh nanoparticles by acting as a "bridge"; Zhao et al.[45] suggested that GO can function as a dispersing agent and significantly enhance the dispersion of the coexisting Gth by heteroaggregation. As such, we expect that CNM with varied sizes and morphologies might exert diverse effects on the phase transformation of Fh.

This work aims to investigate the effects of the omnipresent nanoparticles on the transformation of Fh by selecting CNM (i.e., PHF and GO) as representatives. The transformation kinetics of Fh, the composition and morphologies of the products, and the related reaction mechanisms were investigated. The results of this study may provide novel information for clarifying the phase transformation behavior of Fh and shed new light on understanding the diverse effects of the naturally or artificially produced nanomaterials on natural minerals.

2. EXPERIMENTAL SECTION

2.1. Materials. GO was prepared by oxidizing graphite using a modified Hummers' method,[46] and the specific oxidation process is described in the Supporting Information (Page S3). High-purity (99%) PHF ($C_{60}(OH)_{21}\cdot 6H_2O$) was obtained from Suzhou Dade Carbon Nanotechnology Company, Ltd, China. $Fe(NO_3)_3\cdot 9H_2O$, NaOH, ammonium oxalate, HNO_3, and HCl of analytical grade (>99%) were obtained from Guangzhou Chemical Reagent Factory, China, and were used without further treatments.

2.2. Synthesis of Fh and the Mixed Samples. Fh was synthesized according to the method used by Cornell and Schwertzmann with slight modifications.[1] In brief, 1 M $Fe(NO_3)_3\cdot 9H_2O$ and 3 M NaOH were simultaneously titrated to pH ∼7 under vigorous magnetic stirring.[24] Then, the obtained Fh was centrifuged and subsequently washed with ultrapure water at 8000 rpm for 10 min (3 times) to remove impurities. To prepare the CNM−Fh dispersion, different concentrations of CNM were respectively mixed with fresh Fh at pH ∼7 and 25 °C to ensure the mass ratio of CNM/Fh = 0, 0.02, or 0.05 (respectively denoted as Fh, 2% GO−Fh, 5% GO−Fh, 2% PHF−Fh, and 5% PHF−Fh). Then, all of the mixtures were continuously stirred for 48 h in closed containers to ensure the well-mixing of CNM and Fh, and the mixing process did not induce the phase transformation of Fh.[47,48]

2.3. Transformation Experiments for Fh and CNM−Fh. Transformation experiments were conducted in closed 250 mL polypropylene bottles for 30 days at 75 °C.[11] The pH of these systems was checked and adjusted (using minimum volumes of 0.1 M NaOH and 0.1 M HNO_3) every day during the first 5 days, at 2 day intervals in days 6−9, and then adjusted every 5 days over the remaining aging time. 25 mL of the dispersions were respectively collected from the bottles after 0, 1, 2, 5, 9, 15, and 30 days to study the transformation kinetics of Fh. The collected samples were centrifuged at 8000 rpm for 10 min to remove the supernatant, and the obtained samples were freeze-dried and stored in dark at 4 °C for further solid phase characterization and chemical analysis. Solution pH was controlled at 7(±0.5) and the temperature was maintained at 75(±1) °C for the following reasons: (1) pH 7 is environmentally relevant; and (2) 75 °C enabled the transformation reaction in a reasonable and controllable length of time.[11,12]

2.4. Characterization Methods. X-ray diffraction (XRD) was used to verify the mineral and CNM phases during the 30 day period; the analyses were conducted on a Bruker D8 ADVANCE X-ray diffractometer (Karlsruhe, Germany) using Cu Kα radiation operating at 40 kV and 40 mA. The patterns were recorded over a 2θ range of 10−70° at a scan speed of 3°/min.

The relative chemical contents and the oxidation degree of the three types of CNM were characterized by X-ray photoelectron spectroscopy (XPS, Thermo Fisher Scientific K-Alpha). The samples for the XPS analysis were prepared by pressing the sample powders to slice at room temperature. The analysis of the obtained spectra was conducted using the Avantage program.[49]

The zeta potentials of the samples were measured using a Zetasizer Nano ZS90 instrument. 0.1 g of each sample was dispersed in ultra-water, and the pH of the suspensions was adjusted ranging from 4 to 10 using 0.1 M HNO_3 and 0.1 M NaOH solutions.

Atomic force microscopy (AFM) images of the samples were obtained before aging using a Bruker Multimode AFM controlled by a Nanoscope V controller using a tapping mode. The particle sizes of the samples (i.e., Fh, 5% PHF−Fh, and

https://dx.doi.org/10.1021/acsearthspacechem.9b00261
ACS Earth Space Chem. 2020, 4, 335−344

5% GO−Fh) were measured by the protrusion height observation on mica substrates. A drop of highly diluted aqueous suspension of samples was added on mica plates, and then, the sample was fully air-dried for AFM characterization using a tapping mode.[48]

The transformation kinetics of Fh in the presence of CNM was further investigated by dissolving the collected samples with acid/ammonium oxalate (at pH = 3) in the absence of light for 4 h, according to previous works.[50,51] The ratio of Fe_o/Fe_t was used to represent the transformation kinetics of Fh, where Fe_o was the oxalate-soluble iron (i.e., the untransformed Fh) and Fe_t was the content of total Fe that was dissolved by 6 M HCl.[22,51] The content of Fe was measured by atomic absorption spectroscopy.

^{57}Fe Mössbauer spectroscopy (MS) was used at room temperature in the transmission mode operating in constant acceleration mode using a Silver Double Limited WSS-10 spectrometer. A ^{57}Co in the Rh matrix was used as the Mössbauer source. The velocity drive transducer was operated in a triangular waveform mode over energy ranges of ±15 mm/s. The spectrometer was calibrated using standard α-Fe foil. To prepare the test, 10 mg of each sample was uniformly placed in the holder and measured at room temperature (298 K). The obtained spectra were quantitatively analyzed with the MossWinn program.[52] The spectra were deconvoluted based on the least square fitting of the Lorentzian line-shaped profile, and the subspectra attributed to different phases were classified on the basis of their hyperfine parameters [i.e., isomer (IS), quadrupole splitting (QS), and magnetic hyperfine field (B_{HF})]. The proportion of each phase was determined according to the area of its corresponding subspectrum.[53]

Scanning electron microscopy (SEM) images were obtained using a ZEISS Supra 55 field emission SEM in the high vacuum mode with a voltage of 30 kV. The morphologies of the transformed products after aging for 30 days were observed. Transmission electron microscopy (TEM) and high-resolution TEM (HRTEM) images of the transformed products after aging for 30 days were obtained by an FEI Talos F200S instrument operating at 200 kV. The collected samples were uniformly dispersed in distilled water by ultrasonic treatment. Then, a drop of the suspension was placed on a holey silicon nitride film TEM grid and was air-dried for further characterization.

3. RESULTS AND DISCUSSION

3.1. Characterization of CNM, Fh, and Fh−CNM before Transformation. In the XRD patterns (Figure S1A), the characteristic (001) reflection of GO (2θ = 11°) were noticeable,[54] while only a broad reflection of PHF was observed at 2θ range of 20−35°, identifying its weak crystalline structure.[55,56] XPS results showed that the CNM contained a large percentage of oxygen (31.3% for GO and 28.8% for PHF) (Figure S1B), suggesting the high oxidation ratio of the CNM. The XRD patterns of Fh and CNM−Fh samples before aging were collected (Figure S2). Two broad reflections at 2θ = 35 and 63° for Fh indicated that the obtained sample was two-line Fh.[48,57] The small amount of coexisting CNM (no more than 5%) did not influence the XRD reflections of Fh, suggesting that the crystal structure of Fh was conserved in the CNM−Fh mixture before the aging experiments.

The zeta potential of Fh and CNM was determined (Figure 1). The pH_{zpc} of Fh was ∼8, and the zeta potentials of the CNM were all below −30 mV at pH = 7, in agreement with previous studies.[42,58] At the pH of our experiments (pH = 7), Fh was positively charged while the CNM was negatively charged, suggesting strong electrostatic interactions between Fh and CNM. In addition to electrostatic interaction, Liu et al.[42] suggested that chemical bonds could form between Fh and PHF through the dehydroxylation of PHF and deprotonation of Fh. GO with abundant hydroxyl groups (e.g., −OH) may interact with Fh through similar mechanisms. The strong interaction between Fh and CNM could affect the aggregation and dispersion of Fh (as proved by the following sedimentation and AFM experiments), which may further influence the phase transformation process of Fh.

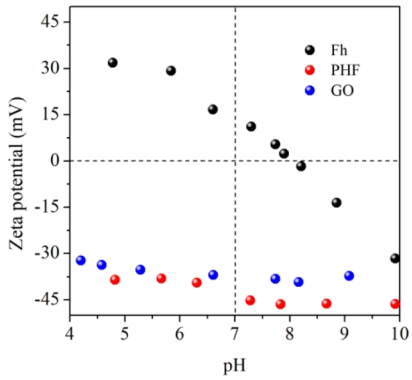

Figure 1. Zeta potentials of CNM and Fh under different pH conditions. Fh is positively charged at pH = 7, while the CNM are all highly negatively charged, suggesting that Fh can interact with Fh by electrostatic attraction.

The sedimentation of Fh and Fh−CNM samples were tested to examine the effect of CNM on the aggregation/dispersion of Fh (Figure S3). The suspended particles settled in both the Fh and Fh−PHF systems after 10 min, with the former system showing slightly larger sediment volume, which suggested that PHF could accelerate the sedimentation of Fh. While in the Fh−GO system, no obvious sedimentation of the particles was observed after 10 min, and a large volume of sample was retained in the suspension even after 30 d. Thus, the presence of GO can significantly enhance the dispersion (i.e., inhibit the aggregation) of Fh particles. Zhao et al.[45] also found that GO could enhance the dispersion of Gth particles, due to the excellent dispersibility of GO in water, which then led to slow sedimentation of the GO−Gth mixture. We believe GO has a similar effect on Fh particles in the Fh−GO system. As such, although CNM may have strong interactions with Fh, they show quite different effects on the aggregation/dispersion of Fh particles.

The AFM results further supported the above hypothesis. The micrometer-sized GO sheet showed a thickness of ∼0.5 nm, with some wrinkles on the sheet (Figure S1C). The granular PHF and Fh showed a single particle size of ∼1.5 and 2−3 nm, respectively (Figures S1D and 2A). As for the GO−Fh mixture (Figure 2B), Fh aggregates, with an average size of ∼15 nm, were mostly dispersed on the edges of GO, with a small amount located on the planar surface of GO. The abundance of highly reactive groups on the edge of GO should have strong interactions with Fh, enabling the association of GO with Fh particles at these sites. For the mixture of PHF−Fh (Figure 2C), the sizes of the aggregates were over 100 nm, indicating the aggregation of PHF and Fh particles was significant. The AFM results by Xu et al.[48] and Liu et al.[42] also found that PHF can enhance the aggregation of Fh. These

https://dx.doi.org/10.1021/acsearthspacechem.9b00261
ACS Earth Space Chem. 2020, 4, 335−344

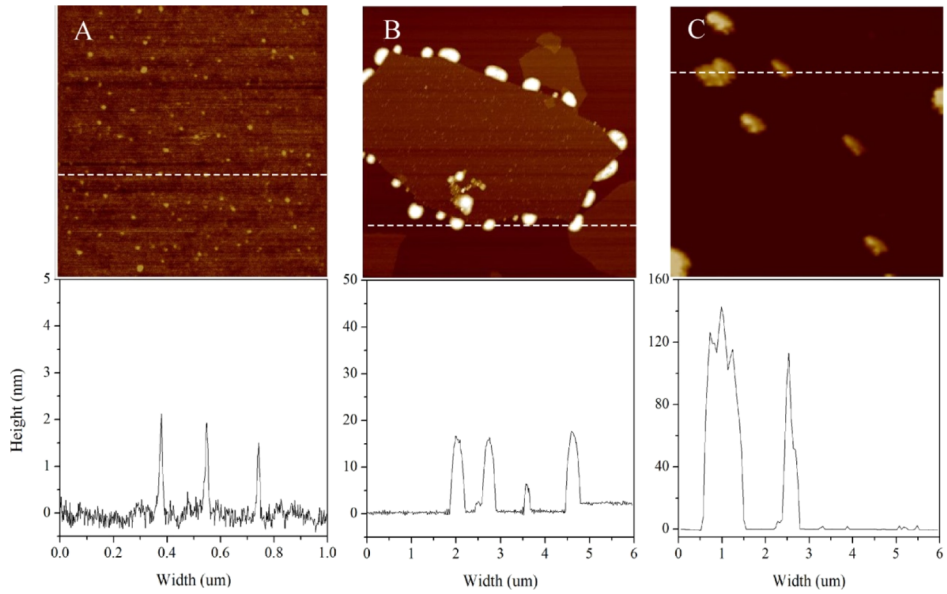

Figure 2. AFM height images of samples before aging (A) Fh, (B) 5% GO−Fh, and (C) 5% PHF−Fh. GO dispersed Fh, while PHF accelerated Fh aggregation.

AFM results, in combination with the above sedimentation results, indicated that the large lamellar GO could disperse Fh particles, while PHF could enhance the aggregation of Fh.

Taken together, the above characterization results demonstrated that CNM has relatively strong interactions with Fh particles, due to their oppositely charged surfaces and highly reactive surface groups. In addition, because of their different surface morphologies, GO could disperse Fh, while PHF accelerated the aggregation of Fh. Accordingly, these CNM might have quite different effects on the transformation of Fh.

3.2. Transformation Process and the Products of Fh.

3.2.1. XRD Characterization Results. The XRD patterns of the collected samples during the aging process were obtained, and the characteristic reflections of both Hem and Gth were determined, in all of the systems (Figure 3). In the Fh system, both Hem and Gth formed simultaneously during the transformation reaction, with Hem being the major product. In a similar study, Das et al.[15] investigated the effect of pH and temperature on the transformation of Fh, and they also found a high Hem/Gth ratio for the samples collected from the system with neutral pH and high temperature (e.g., 100 °C). We also noticed that the intensity of the characteristic reflections of Hem and Gth emerged within the first 5 days, and then remained relatively constant with continuous aging, which suggested that most of the Fh should have transformed within the 5 day window under this aging condition (pH = 7, 75 °C).

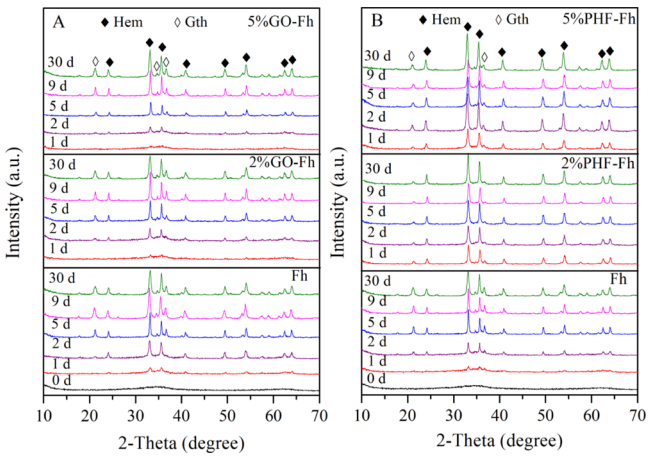

Figure 3. XRD patterns of the products during the transformation of Fh in the presence of varying mass ratios of CNM−Fh: the effects of (A) GO and (B) PHF on the transformation of Fh: the transformed products were mainly Hem with a small amount of Gth. GO inhibited the transformation of Fh, while PHF accelerated the transformation process.

In the GO−Fh systems, XRD characterization recorded much stronger characteristic reflections belonging to Hem than to Gth (Figure 3A). In addition, the intensities of the characteristic reflections of both Hem and Gth were clearly weakened in comparison with the Fh system, and this phenomenon was more obvious with the increase of GO content. For example, after the first day's reaction, the characteristic reflections of Hem, which were noticeable in the Fh system and in the 2% GO−Fh system, became undetectable in the 5% GO−Fh system. These results suggest that the transformation process of Fh was evidently inhibited by GO.

In the PHF−Fh systems, Hem is also the main transformed products. Interestingly, PHF evidently accelerated the transformation rate, particularly at high PHF content (Figure 3B). As compared with those in the Fh system, much stronger reflections of Hem in combination with weak reflections of Gth could be detected after the first day in the presence of PHF. Moreover, with increasing the content of PHF, the transformation rate of Fh became much faster. The reflections of Hem and Gth in the 5% PHF−Fh system retained nearly unchanged after 2 days, suggesting a very quick transformation process of Fh (mostly within 2 days). It was also noticeable that the Gth reflection intensity in the 5% PHF−Fh was weaker than that in the Fh system, suggesting an inhibited effect of PHF on Fh transformation to Gth.

The XRD characterization results above showed well that different CNM can have quite obvious and unique effects on the transformation of Fh. Previous studies also showed that the

https://dx.doi.org/10.1021/acsearthspacechem.9b00261
ACS Earth Space Chem. 2020, 4, 335−344

transformation rate and the transformed products of Fh were closely related to the coexisting substances.[1] For instance, clay minerals inhibited the transformation of Fh and favored the formation of Hem; reducing agents [e.g., Fe(II)] evidently accelerated the transformation of Fh to Gth.[19,26]

3.2.2. Transformation Kinetics Analysis. To quantify the transformation kinetics of Fh in the systems with or without CNM, the untransformed Fh in the system was determined using the acid/ammonium oxalate dissolution method.[1,22,51] The obtained dissolution kinetics (Figure 4A) showed that

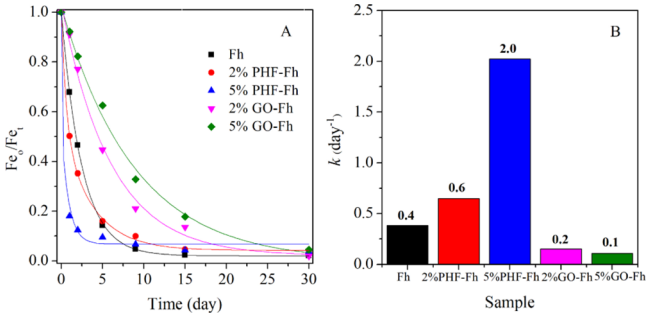

Figure 4. (A) Fe_o/Fe_t (a measure of the transformation of Fh) vs time. Fe_o: the concentration of Fe dissolved in ammonium oxalate; Fe_t: the concentration of Fe dissolved in HCl (6 M). (B) Rate of the transformation of the samples. PHF evidently accelerated Fh transformation, whereas GO inhibited the transformation of Fh.

most of the Fh (nearly 83%) were transformed within 5 days in the Fh system while approximately 15 days were needed to reach a similar extent of Fh transformation in the 5% GO−Fh system, and only 2 days were required in the 5% PHF−Fh system. In addition, the effects of CNM became more evident at higher CNM−Fh ratio. Das et al.[59] studied the effects of arsenate on the transformation rate of Fh at pH = 10, and they found that the transformation rate decreased as As/Fe increased. Hence, the type and abundance of a coexisting substance are both important factors affecting the transformation of Fh.

The percentages of remaining Fh in the systems were fitted with the first-order kinetics model (1)[59]

$$[A]_t = [A]_0\, e^{-kt} \quad (1)$$

where k is a rate constant, t is the reaction time, $[A]_t$ is the amount of remaining Fh at time t, and $[A]_0$ is the initial amount of Fh before aging. This model fits the kinetic data well (R^2 > 99%). The rate constant of Fh in the control system was determined to be 0.4/day (Figure 4B), comparable with the value reported by Das et al.[15] [0.329 (±0.096)/day under the condition of pH = 7 and 75 °C], which was calculated from the integrated intensities of the XRD characteristic reflections of Hem and Gth. In the PHF−Fh system with 5% PHF−Fh, the rate constant reached a value of 2.0/day, nearly five times faster than that observed in the Fh system. As for the GO−Fh system with 5% GO−Fh, the rate constant decreased to 0.1/day, only about one-fourth of the value obtained for the Fh system. The transformation kinetics determined here are consistent with the above results obtained by XRD characterization, and together they demonstrate that the coexisting CNM can influence the transformation of Fh (i.e., inhibition by GO and acceleration by PHF).

3.3. Determination of Hem/Gth Ratio in the Final Products by Mössbauer Spectra. The results above indicated that Fh almost completely transformed into Hem/Gth after 30 days in all of the systems. Here, MS was employed to further quantify the relative content of Hem and Gth in the final products (Figure 5), with the purpose of further investigating the different effects of various CNM on the transformation of Fh. The obtained product from the Fh system was fitted to two sextets (Figure 5A), and the relevant parameters were obtained (Table 1). The values of IS, QS, and B_{HF} of the two sextets were respectively consistent with the parameters of Hem (IS = 0.37 mm/s, QS = −0.20 mm/s, and B_{HF} = 51 T) and Gth (IS = 0.37 mm/s, QS = −0.26 mm/s, and B_{HF} = 37 T), suggesting the formation of Hem and Gth in the products, in agreement with previous studies.[1,60] The relative areas of the fitted spectra arising from Hem and Gth in the ^{57}Fe MS spectra were also determined to obtain an estimate of the relative abundance of Hem and Gth in the sample (Table 1). The calculated relative area belonging to Hem and Gth was 63.2 and 36.8, respectively, indicating that the relative ratio of Hem/Gth was ∼1.7 (=63.2/36.8) and that Hem was the main mineral phase in the transformed product. This finding was consistent with our XRD analyses (above), which also indicated that Hem was the main product after transformation.

For the system containing CNM, each spectrum was also fitted with two sextets (Figure 5B,C). Then, the relative areas belonging to Hem and Gth were obtained (Table 1), which showed that the presence of 5% GO had no obvious effect on the relative content of Hem and Gth (Hem/Gth = 63.7/36.3), as compared with the pure Fh system (1.8 vs 1.7). As for the sample obtained from the 5% PHF−Fh system, the relative content of Hem and Gth (Hem/Gth = 78.9/21.1) was much higher than that in the pure Fh system (3.7 vs 1.7), indicating

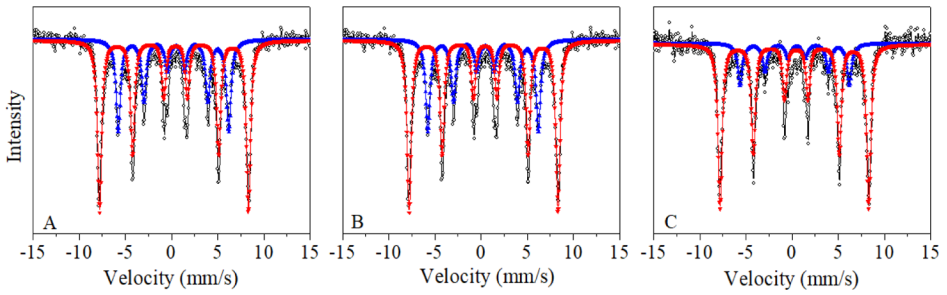

Figure 5. ^{57}Fe Mössbauer spectra of the transformed products recorded at room temperature. (A) Product of Fh, (B) product of 5% GO−Fh, and (C) product of 5% PHF−Fh. Red line: Hem, blue line: Gth. The content of Gth was lower in the 5% PHF−Fh system, in comparison with those in the other two systems.

https://dx.doi.org/10.1021/acsearthspacechem.9b00261
ACS Earth Space Chem. 2020, 4, 335−344

Table 1. Room Temperature Mössbauer Fitting Parameters of Different Samples (IS: Isomer Shift, QS: Quadrupole Splitting, and B_{HF}: Internal Hyperfine Splitting). GO Has No Obvious Influence on the Product Type, While PHF Favors the Transformation of Fh to Hem

sample	signal	IS (mm/s)	QS (mm/s)	B_{HF} (T)	relative area (%)	affiliation
Fh-30	sextet	0.37	−0.18	50.3	63.2	hematite
	sextet	0.37	−0.26	37.4	36.8	goethite
5% GO−Fh-30	sextet	0.37	−0.17	50.1	63.7	hematite
	sextet	0.36	−0.26	37.2	36.3	goethite
5% PHF−Fh-30	sextet	0.37	−0.21	50.0	78.9	hematite
	sextet	0.41	−0.21	36.8	21.1	goethite

that PHF could promote the transformation of Fh to Hem over Gth. The MS result is consistent with our XRD results (Figure 3B), which also indicated that the final product in the 5% PHF−Fh system had weaker characteristic Gth reflections. The formation of Hem promoted by PHF may be caused by the enhanced aggregation of Fh particles by PHF, as Hem was formed through the aggregation and dehydration pathway, while Gth may be formed preferentially through the dissolution−recrystallization pathway.[2,61]

3.4. Microscopic Analysis of the Aged Products. SEM and TEM were used to observe the sizes and morphologies of the transformed products after being aged for 30 days. The average particle sizes (As) of the products were obtained by measuring 50 particles by SEM (Figure S4), which clearly showed that PHF caused the formation of larger product particles (compared with that in the Fh system), whereas GO showed no obvious effect on the particle size of the transformed product. The TEM images of the aged products in the pure Fh system showed some rhombic particles with a length of 30−40 nm and a width of 20−30 nm (Figure 6A), which were comparable to the As value of the product (38 nm) in the pure Fh system observed by SEM (Figure S4A). Fast Fourier transformation of the HRTEM images showed that the plane distances of the rhombic particles in the aged product of Fh were 2.2 and 2.7 Å, which were in accordance with the (113) and (104) planes of Hem, respectively.[62,63] In addition, rod-like particles with a length of 50−60 nm (Figure 6A) were also observed in the product, and the typical plane distances of 4.2 Å can be assigned to the (110) plane of Gth.[64,65] These TEM results further supported the above XRD results, confirming the formation of both Hem and Gth in the aged products.

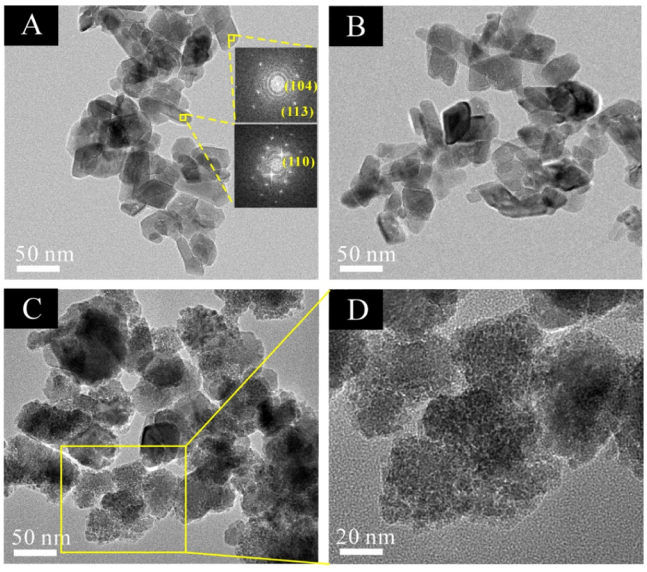

Figure 6. TEM images of the transformed products: (A) Fh-30, Hem are rhombic particles and Gth are acicular-shape particles; (B) 5% GO−Fh-30, GO shows no evident effect on the morphology and size of the transformation product; (C) 5% PHF−Fh-30, Hem particles are larger than the other systems; and (D) enlarged area of C.

With respect to the aged products from the GO−Fh system, quite a similar particle size (As = 40 nm) and morphology as those from the pure Fh system were observed (Figures 6B and S4B), suggesting that GO showed no evident impact on the size and morphology of the product. Interestingly, the aged products from the PHF−Fh system showed a larger particle size (As = 54 nm) and less regular morphology (rhombic-like and round-like particles with rough surfaces), as compared with the samples from the other two systems (Figures 6C,D and S4C). Cornell.[22] indicated that the coexisting sugars could serve as templates and facilitate the aggregation of Fh at pH 10−12, which favored the formation of Hem and also changed the morphology of the final Hem particle (from a prismatic structure to distorted platelets). Herein, the larger particle size and irregular morphology of the products may be attributed to the fast aggregation and transformation of Fh in the presence of PHF, as shown by the characterization results above (Figures 2−4).

The SEM and TEM results showed that GO did not influence the particle size or morphology of the transformed products after 30 days, while PHF both increased the particle size and altered the morphology of the transformed products. These results, in combination with the above XRD and MS results, demonstrated that PHF affected the transformation of Fh more significantly than GO did in terms of both the transformation rate and the particle size and morphology of the products.

3.5. Possible Mechanisms of Fh Transformation with or without CNM. As is well known, the formation of Hem always involves a solid phase transformation process, while the formation of Gth generally needs a dissolution−recrystallization pathway.[1,9] Because Hem is the main transformed product in the tested systems, dissolution of Fh in these systems should not be significant. In addition, XPS results in this study showed that the type and contents (31.3% for GO and 28.8% for PHF) of surface functional groups (C−OH) on PHF and GO are quite similar, so that they will not have much different effects on the dissolution of Fh (as the formation of strong C−O−Fe chemical bonds should be the main reason causing the dissolution of Fh). As such, the different effects of these CNM on the phase transformation of Fh should be mainly caused by influencing its aggregation or dispersion, rather than influencing the dissolution of Fh (schematic diagram in Figure 7). Actually, a number of previous studies showed that the

https://dx.doi.org/10.1021/acsearthspacechem.9b00261
ACS Earth Space Chem. 2020, 4, 335−344

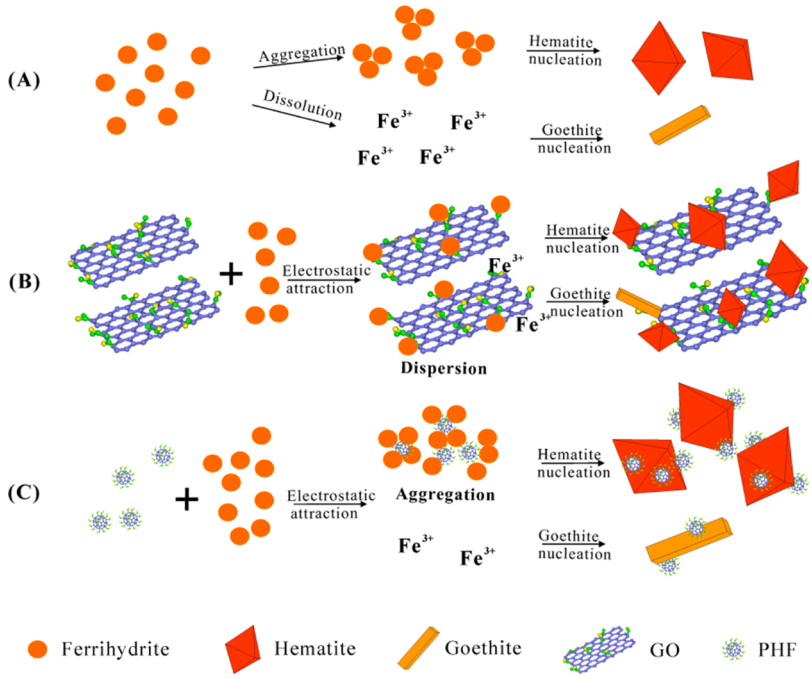

Figure 7. Schematic drawing of the transformation processes of Fh to Hem/Gth in different systems. (A) Transformation process in the Fh system, (B) transformation process in the GO−Fh system, and (C) transformation process in the PHF−Fh system.

coexisting small substances (e.g., ions and organic matter) can inhibit the aggregation and/or direct contact of Fh particles by covering the surface active sites of Fh, whereas the clay minerals usually disperse Fh particles by acting as "barriers". In both cases, the transformation process of Fh will be inhibited.[12,24,66] In this sense, the evidently different effects of the CNM on the dispersion and aggregation of Fh should also lead to the various transformation processes and rates of Fh transformation.

In the control system, as the Fh nanoparticles possess high surface energy, they tend to aggregate to minimize interfacial energy.[1] Besides, Weatherill et al.[67] indicated that as the solution pH approaches the pH_{zpc} of Fh (pH ∼8), the repulsive electrostatic interactions would gradually decrease while the importance of van der Waals forces increases. As such, Fh nanoparticles could aggregate at pH = 7. Moreover, the high reaction temperature (75 °C) favored the dehydration of Fh. Here, the formation of Hem was favored under this aging condition as the transformation of Fh into Hem is a solid phase transformation process (via aggregation and dehydration). On the other hand, a small amount of Gth was observed in the product, which should be caused by the dissolution and recrystallization of Fh.[68,69]

According to the results from XPS and zeta potential characterization, GO could well disperse in solution because of its abundant surface functional groups (e.g., −OH) and highly negative charge at pH = 7. Actually, a previous study showed that GO could function as a dispersing agent to disperse positively charged nanoparticles (e.g., Gth).[45] In this study, the negatively charged GO could interact with Fh particles through electrostatic attraction and chemical bonding in the mixing process before aging. Simultaneously, by acting as a dispersing agent, GO can also disperse the Fh nanoparticles and inhibit the direct contact and attachment of the Fh nanoparticles by functioning as a "barrier" because of its large (relative to Fh nanoparticles) lamellar shape. As the transformation of Fh to Hem is an aggregation, rearrangement, and dehydration process, the direct contact of Fh particles is the essential prerequisite. Therefore, the transformation of Fh to Hem is evidently slowed down in the GO−Fh system. Similar dispersing and separating effects of Fh particles were also observed in the systems with clay mineral lamella, which also slowed down the transformation rate of Fh.

In the PHF−Fh system, the negatively charged PHF could interact with positively charged Fh and neutralize its surface charges, which favors the formation of large PHF−Fh aggregates. More importantly, as PHF possesses a comparable particle size (∼1.5 nm) with Fh and have rigid round shapes, it acts as a "bridge" to enhance the direct contact of Fh particles,[42] which subsequently can accelerate the transformation of Fh to Hem and also lead to the formation of larger sized Hem particles. This is quite different from the situations in the systems with small coexisting substances (e.g., ions and molecules). For example, although the coexisting sugar can help in enhancing the aggregation of Fh particles under alkaline conditions, it will also cover a large part of the Fh surface, which would subsequently inhibit the direct contact between Fh particles and further reduce the transformation rate of Fh.[22] Additionally, the relatively faster formation of Hem may lead to a higher ratio of Hem/Gth, as compared with the situations in the Fh and GO−Fh systems.

We also noticed that because of the large difference in the particle sizes of the two components in the GO−Fh system, Fh aggregates could only partly contact with GO during the transformation process (above AFM and SEM results), which suggests that the rest of the large part of the aggregates will not be as affected by GO during the transformation process. This should explain the similarity of the transformation products (e.g., Hem/Gth ratio, the particle size, and the morphologies) in the Fh system and the GO−Fh system. While in the PHF−Fh system, these two components can contact closely because of their comparable particle size and strong interactions, and

https://dx.doi.org/10.1021/acsearthspacechem.9b00261
ACS Earth Space Chem. 2020, 4, 335−344

subsequently, a change in the particle size and morphology of the transformed products (compared with the Fh system) occurs.

4. CONCLUSIONS AND IMPLICATIONS

This study, for the first time, investigated the effects of CNM on the phase transformation of Fh. Although the tested CNM contained similar elemental composition and surface groups, they showed significantly different effects on the transformation process. Of particular interest is the effect of PHF, which not only accelerated the transformation rate of Fh but also changed the Hem/Gth ratio, as well as the particle size and morphology of the final products. The results of this study showed that the coexisting nanoparticles can significantly affect the transformation process of Fh mainly by changing the aggregation and contact of Fh particles. In this sense, we believe that the ubiquitously present nanoparticles in the environment, which may differ in chemical composition, surface groups, particle size, morphology, and so forth, will have more diverse effects on the transformation process of Fh. It is worth noting that the environmental conditions (e.g., pH, temperature, and coexisting substances) can also affect the interaction between Fh and the coexisting nanoparticles, which may further affect the phase transformation of Fh. More detailed studies involving the effects of nanoparticles on the transformation of Fh under different environmental conditions are needed in the future.

■ ASSOCIATED CONTENT

Supporting Information

The Supporting Information is available free of charge at https://pubs.acs.org/doi/10.1021/acsearthspacechem.9b00261.

XRD, XPS, and AFM patterns of CNM; modified Hummers' methods; XRD patterns of Fh and CNM−Fh mixed samples before aging; sedimentation conditions of Fh, 5% GO−Fh, and 5% PHF−Fh before aging; SEM images of the aged products of Fh, 5% GO−Fh, and 5% PHF−Fh (PDF)

■ AUTHOR INFORMATION

Corresponding Author

Runliang Zhu − *CAS Key Laboratory of Mineralogy and Metallogeny/Guangdong Provincial Key Laboratory of Mineral Physics and Materials, Guangzhou Institute of Geochemistry and Institutions of Earth Science, Chinese Academy of Sciences, Guangzhou 510640, China;* orcid.org/0000-0002-7591-6625; Phone: +86-020-85297603; Email: zhurl@gig.ac.cn

Authors

Lixia Yan − *CAS Key Laboratory of Mineralogy and Metallogeny/Guangdong Provincial Key Laboratory of Mineral Physics and Materials, Guangzhou Institute of Geochemistry and Institutions of Earth Science, Chinese Academy of Sciences, Guangzhou 510640, China; University of Chinese Academy of Sciences, Beijing 100049, China*

Jing Liu − *CAS Key Laboratory of Mineralogy and Metallogeny/Guangdong Provincial Key Laboratory of Mineral Physics and Materials, Guangzhou Institute of Geochemistry and Institutions of Earth Science, Chinese Academy of Sciences, Guangzhou 510640, China*

Yixuan Yang − *CAS Key Laboratory of Mineralogy and Metallogeny/Guangdong Provincial Key Laboratory of Mineral Physics and Materials, Guangzhou Institute of Geochemistry and Institutions of Earth Science, Chinese Academy of Sciences, Guangzhou 510640, China; University of Chinese Academy of Sciences, Beijing 100049, China*

Jianxi Zhu − *CAS Key Laboratory of Mineralogy and Metallogeny/Guangdong Provincial Key Laboratory of Mineral Physics and Materials, Guangzhou Institute of Geochemistry and Institutions of Earth Science, Chinese Academy of Sciences, Guangzhou 510640, China;* orcid.org/0000-0002-9002-4457

Hongjuan Sun − *Southwest University of Science and Technology, Mianyang, Sichuan 621010, China*

Hongping He − *CAS Key Laboratory of Mineralogy and Metallogeny/Guangdong Provincial Key Laboratory of Mineral Physics and Materials, Guangzhou Institute of Geochemistry and Institutions of Earth Science, Chinese Academy of Sciences, Guangzhou 510640, China*

Complete contact information is available at: https://pubs.acs.org/10.1021/acsearthspacechem.9b00261

Notes

The authors declare no competing financial interest.

■ ACKNOWLEDGMENTS

The authors acknowledge Chakraborty, S., and reviewers for their comments and suggestions which greatly improved this paper. This is contribution No. IS-2828 from GIGCAS. This work was supported by the National Natural Science Foundation of China (grant no. 41872044, 41902040), and Youth Innovation Promotion Association CAS (grant no. 2020347).

■ REFERENCES

(1) Cornell, R. M.; Schwertmann, U. *The Iron Oxides : Structure, Properties, Reactions, Occurences and Uses*; Wiley-VCH, 2003.

(2) Brinza, L.; Hong, P. V.; Shaw, S.; Mosselmans, J. F. W.; Benning, L. G. Effect of Mo and V on the hydrothermal crystallization of hematite from ferrihydrite: an in situ energy dispersive X-ray diffraction and X-ray absorption spectroscopy study. *Cryst. Growth Des.* **2015**, *15*, 4768−4780.

(3) Lu, Y.; Hu, S.; Wang, Z.; Ding, Y.; Lu, G.; Lin, Z.; Dang, Z.; Shi, Z. Ferrihydrite transformation under the impact of humic acid and Pb: kinetics, nanoscale mechanisms, and implications for C and Pb dynamics. *Environ. Sci.: Nano* **2019**, *6*, 747−762.

(4) Cismasu, A. C.; Michel, F. M.; Stebbins, J. F.; Levard, C.; Brown, G. E., Jr Properties of impurity-bearing ferrihydrite I. Effects of Al content and precipitation rate on the structure of 2-line ferrihydrite. *Geochim. Cosmochim. Acta* **2012**, *92*, 275−291.

(5) Dai, C.; Lin, M.; Hu, Y. Heterogeneous Ni- and Cd-bearing ferrihydrite precipitation and recrystallization on quartz under acidic pH condition. *ACS Earth Space Chem.* **2017**, *1*, 621−628.

(6) Dai, C.; Liu, J.; Hu, Y. Impurity-bearing ferrihydrite nanoparticle precipitation/deposition on quartz and corundum. *Environ. Sci.: Nano* **2018**, *5*, 141−149.

(7) Perez, J. P. H.; Tobler, D. J.; Thomas, A.; freeman, h.; Dideriksen, K.; Radnik, J.; Benning, L. G. Adsorption and reduction of arsenate during the Fe^{2+}-induced transformation of ferrihydrite. *ACS Earth Space Chem.* **2019**, *3*, 884.

(8) Soltis, J. A.; Feinberg, J. M.; Gilbert, B.; Penn, R. L. Phase Transformation and particle-mediated growth in the formation of hematite from 2-line ferrihydrite. *Cryst. Growth Des.* **2016**, *16*, 922−932.

(9) Vodyanitskii, Y. N.; Shoba, S. A. Ferrihydrite in soils. *Eurasian Soil Sci.* **2016**, *49*, 796−806.
(10) Alvarez, M.; Sileo, E. E.; Rueda, E. H. Effect of Mn(II) incorporation on the transformation of ferrihydrite to goethite. *Chem. Geol.* **2005**, *216*, 89−97.
(11) Vu, H. P.; Moreau, J. W. Thiocyanate adsorption on ferrihydrite and its fate during ferrihydrite transformation to hematite and goethite. *Chemosphere* **2015**, *119*, 987−993.
(12) Das, S.; Essilfie-Dughan, J.; Hendry, M. J. Fate of adsorbed arsenate during phase transformation of ferrihydrite in the presence of gypsum and alkaline conditions. *Chem. Geol.* **2015**, *411*, 69−80.
(13) Kennedy, C. B.; Scott, S. D.; Ferris, F. G. Hydrothermal phase stabilization of 2-line ferrihydrite by bacteria. *Chem. Geol.* **2004**, *212*, 269−277.
(14) Hua, J.; Liu, C.; Li, F.; Zhu, Z.; Wei, Z.; Chen, M.; Gao, T.; Qiu, G. Effects of rare earth elements' physicochemical properties on their stabilization during the $Fe(II)_{aq}$-induced phase transformation of ferrihydrite. *ACS Earth Space Chem.* **2019**, *3*, 895.
(15) Das, S.; Hendry, M. J.; Essilfie-Dughan, J. Transformation of two-line ferrihydrite to goethite and hematite as a function of pH and temperature. *Environ. Sci. Technol.* **2011**, *45*, 268−275.
(16) Jiang, Z.; Liu, Q.; Dekkers, M. J.; Vidal, B.; José, T.; Roberts, A. P. Control of Earth-like magnetic fields on the transformation of ferrihydrite to hematite and goethite. *Sci. Rep.* **2016**, *6*, 30395.
(17) Jambor, J. L.; Dutrizac, J. E. Occurrence and constitution of natural and synthetic ferrihydrite, a widespread iron oxyhydroxide. *Chem. Rev.* **1998**, *98*, 2549−2586.
(18) Hansel, C. M.; Learman, D. R.; Lentini, C. J.; Ekstrom, E. B. Effect of adsorbed and substituted Al on Fe(II)-induced mineralization pathways of ferrihydrite. *Geochim. Cosmochim. Acta* **2011**, *75*, 4653−4666.
(19) Schwertmann, U.; Friedl, J.; Stanjek, H.; Schulze, D. G. The effect of clay minerals on the formation of goethite and hematite from ferrihydrite after 16 years' ageing at 25°C and pH 4-7. *Clay Miner.* **2000**, *35*, 613−623.
(20) Chen, C.; Kukkadapu, R.; Sparks, D. L. Influence of coprecipitated organic matter on $Fe^{2+}_{(aq)}$-catalyzed transformation of ferrihydrite: implications for carbon dynamics. *Environ. Sci. Technol.* **2015**, *49*, 10927−10936.
(21) Alvarez, M.; Horst, M. F.; Sileo, E. E.; Rueda, E. H. Effect of Cd(II) on the ripening of ferrihydrite in alkaline media. *Clay Clay Miner.* **2012**, *60*, 99−107.
(22) Cornell, R. M. Effect of simple sugars on the alkaline transformation of ferrihydrite into goethite and hematite. *Clay Clay Miner.* **1985**, *33*, 219−227.
(23) Cornell, R. M.; Schneider, W.; Giovanoli, R. The effect of nickel on the conversion of amorphous iron(III) hydroxide into more crystalline iron oxides in alkaline media. *J. Chem. Technol. Biol.* **2007**, *53*, 73−79.
(24) Cornell, R. M.; Giovanoli, R.; Schindler, P. Effect of silicate species on the transformation of ferrihydrite into goethite and hematite in alkaline media. *Clay Clay Miner.* **1987**, *35*, 21−28.
(25) Liu, C.; Zhu, Z.; Li, F.; Liu, T.; Liao, C.; Lee, J.-J.; Shih, K.; Tao, L.; Wu, Y. Fe(II)-induced phase transformation of ferrihydrite: The inhibition effects and stabilization of divalent metal cations. *Chem. Geol.* **2016**, *444*, 110−119.
(26) Yee, N.; Shaw, S.; Benning, L. G.; Nguyen, T. H. The rate of ferrihydrite transformation to goethite via the Fe(II) pathway. *Am. Mineral.* **2006**, *91*, 92−96.
(27) Cornell, R. M.; Schneider, W. Formation of goethite from ferrihydrite at physiological pH under the influence of cysteine. *Polyhedron* **1989**, *8*, 149−155.
(28) Banfield, J. F.; Zhang, H. Nanoparticles in the environment. *Rev. Mineral. Geochem.* **2001**, *44*, 1−58.
(29) Hochella, M. F.; Mogk, D. W.; Ranville, J.; Allen, I. C.; Luther, G. W.; Marr, L. C.; McGrail, B. P.; Murayama, M.; Qafoku, N. P.; Rosso, K. M. Natural, incidental, and engineered nanomaterials and their impacts on the Earth system. *Science* **2019**, *363*, eaau8299.
(30) Janković, N. Z.; Plata, D. L. Engineered nanomaterials in the context of global element cycles. *Environ. Sci.: Nano* **2019**, *6*, 2697.
(31) Zaytseva, O.; Neumann, G. Carbon nanomaterials: production, impact on plant development, agricultural and environmental applications. *Chem. Biol. Technol. Agric.* **2016**, *3*, 17.
(32) Jariwala, D.; Sangwan, V. K.; Lauhon, L. J.; Marks, T. J.; Hersam, M. C. Carbon nanomaterials for electronics, optoelectronics, photovoltaics, and sensing. *Chem. Soc. Rev.* **2013**, *42*, 2824−2860.
(33) Saxena, M.; Maity, S.; Sarkar, S. Carbon nanoparticles in "biochar" boost wheat (Triticum aestivum) plant growth. *RSC Adv* **2014**, *4*, 39948−39954.
(34) Wang, Y.; Hu, A. Carbon quantum dots: synthesis, properties and applications. *J. Mater. Chem. C* **2014**, *2*, 6921−6939.
(35) Namdari, P.; Negahdari, B.; Eatemadi, A. Synthesis, properties and biomedical applications of carbon-based quantum dots: An updated review. *Biomed. Pharmacother.* **2017**, *87*, 209−222.
(36) De Volder, M. F. L.; Tawfick, S. H.; Baughman, R. H.; Hart, A. J. J. Carbon nanotubes: present and future commercial applications. *Science* **2013**, *339*, 535−539.
(37) Chen, M.; Sun, Y.; Liang, J.; Zeng, G.; Li, Z.; Tang, L.; Zhu, Y.; Jiang, D.; Song, B. Understanding the influence of carbon nanomaterials on microbial communities. *Environ. Int.* **2019**, *126*, 690−698.
(38) DeLuca, T. H.; MacKenzie, M. D.; Gundale, M. J.; Holben, W. E. Wildfire-produced charcoal directly influences nitrogen cycling in ponderosa pine forests. *Soil Sci. Soc. Am. J.* **2006**, *70*, 448−453.
(39) Bieser, J. M. H.; Thomas, S. C. Biochar and high-carbon wood ash effects on soil and vegetation in a boreal clearcut. *Can. J. For. Res.* **2019**, *49*, 1124−1134.
(40) Santín, C.; Doerr, S. H.; Merino, A.; Bucheli, T. D.; Bryant, R.; Ascough, P.; Gao, X.; Masiello, C. A. Carbon sequestration potential and physicochemical properties differ between wildfire charcoals and slow-pyrolysis biochars. *Sci. Rep.* **2017**, *7*, 11233.
(41) Zhao, J.; Wang, Z.; White, J. C.; Xing, B. Graphene in the aquatic environment: adsorption, dispersion, toxicity and transformation. *Environ. Sci. Technol.* **2014**, *48*, 9995−10009.
(42) Liu, J.; Zhu, R.; Xu, T.; Laipan, M.; Zhu, Y.; Zhou, Q.; Zhu, J.; He, H. Interaction of polyhydroxy fullerenes with ferrihydrite: adsorption and aggregation. *J. Environ. Sci.* **2018**, *64*, 1−9.
(43) Cao, H. Q.; Zhu, M. Q.; Li, Y. G. Decoration of carbon nanotubes with iron oxide. *J. Solid State Chem.* **2006**, *179*, 1208−1213.
(44) Lee, S.-H.; Kang, D.; Oh, I.-K. Multilayered graphene-carbon nanotube-iron oxide three-dimensional heterostructure for flexible electromagnetic interference shielding film. *Carbon* **2017**, *111*, 248−257.
(45) Zhao, J.; Liu, F.; Wang, Z.; Cao, X.; Xing, B. Heteroaggregation of graphene oxide with minerals in aqueous phase. *Environ. Sci. Technol.* **2015**, *49*, 2849.
(46) Nethravathi, C.; Rajamathi, M. Chemically modified graphene sheets produced by the solvothermal reduction of colloidal dispersions of graphite oxide. *Carbon* **2008**, *46*, 1994−1998.
(47) Franciscco, P. C. M.; Sato, T.; Otake, T.; Kasama, T. Kinetics of Fe^{3+} mineral crystallization from ferrihydrite in the presence of Si at alkaline conditions and implications for nuclear waste disposal. *Am. Mineral.* **2016**, *101*, 2057−2069.
(48) Xu, T.; Zhu, R.; Liu, J.; Zhou, Q.; Zhu, J.; Liang, X.; Xi, Y.; He, H. Fullerol modification ferrihydrite for the degradation of acid red 18 under simulated sunlight irradiation. *J. Mol. Catal. A: Chem.* **2016**, *424*, 393−401.
(49) Bao, S.; Duan, J.; Zhang, Y. Characteristics of nitric acid-modified carbon nanotubes and desalination performance in capacitive deionization. *Chem. Eng. Technol.* **2018**, *41*, 1793−1799.
(50) Lewis, D. G. Transformations induced in ferrihydrite by oven-drying. *Z. für Pflanzenernährung Bodenkunde* **1992**, *155*, 461−466.
(51) Lin, X.; Burns, R. C.; Lawrance, G. A. Effect of cadmium(II) and anion type on the ageing of ferrihydrite and its subsequent leaching under neutral and alkaline conditions. *Water, Air, Soil Pollut.* **2003**, *143*, 155−177.

(52) Klencsár, Z.; Kuzmann, E.; Vértes, A. User-friendly software for Mössbauer spectrum analysis. *J. Radioanal. Nucl. Chem* **1996**, *210*, 105−118.
(53) Pariona, N.; Camacho-Aguilar, K. I.; Ramos-González, R.; Martinez, A. I.; Herrera-Trejo, M.; Baggio-Saitovitch, E. Magnetic and structural properties of ferrihydrite/hematite nanocomposites. *J. Magn. Magn. Mater.* **2016**, *406*, 221−227.
(54) Chen, C.; Chen, Y.-C.; Hong, Y.-T.; Lee, T.-W.; Huang, J.-F. Facile fabrication of ascorbic acid reduced graphene oxide-modified electrodes toward electroanalytical determination of sulfamethoxazole in aqueous environments. *Chem. Eng. J.* **2018**, *352*, 188−197.
(55) Djordjevic, A.; Nenad, I.; Mariana, S.; Danica, J.; Dragan, U.; Zlatko, R. Synthesis and Characterization of Hydroxyapatite/Fullerenol Nanocomposites. *J. Nanosci. Nanotechnol.* **2015**, *15*, 1538−1542.
(56) Zhang, M.-F.; Xu, Z.-Q.; Ge, Y.-S.; Jiang, F.-L.; Liu, Y. Binding of fullerol to human serum albumin: spectroscopic and electrochemical approach. *J. Photochem. Photobiol., B* **2012**, *108*, 34−43.
(57) Shimizu, M.; Zhou, J.; Schröder, C.; Obst, M.; Kappler, A.; Borch, T. Dissimilatory reduction and transformation of ferrihydrite-humic acid coprecipitates. *Environ. Sci. Technol.* **2013**, *47*, 13375.
(58) Bourlinos, A. B.; Georgakilas, V.; Bakandritsos, A.; Kouloumpis, A.; Gournis, D.; Zboril, R. Aqueous-dispersible fullerol-carbon nanotube hybrids. *Mater. Lett.* **2012**, *82*, 48−50.
(59) Das, S.; Hendry, M. J.; Essilfie-Dughan, J. Effects of adsorbed arsenate on the rate of transformation of 2-line ferrihydrite at pH 10. *Environ. Sci. Technol.* **2011**, *45*, 5557−5563.
(60) Camacho, K. I.; Pariona, N.; Martinez, A. I.; Baggio-Saitovitch, E.; Herrera-Trejo, M.; Perry, D. L. Structural and magnetic properties of the products of the transformation of ferrihydrite: Effect of cobalt dications. *J. Magn. Magn. Mater.* **2017**, *429*, 339−347.
(61) Zhang, D.; Wang, S.; Wang, Y.; Gomez, M. A.; Duan, Y.; Jia, Y. The transformation of two-line ferrihydrite into crystalline products: effect of pH and media (sulfate versus nitrate). *ACS Earth Space Chem.* **2018**, *2*, 577−587.
(62) Li, W.; Liang, X.; An, P.; Feng, X.; Tan, W.; Qiu, G.; Yin, H.; Liu, F. Mechanisms on the morphology variation of hematite crystals by Al substitution: The modification of Fe and O reticular densities. *Sci. Rep.* **2016**, *6*, 35960.
(63) Tadić, M.; Čitaković, N.; Panjan, M.; Stojanović, Z.; Marković, D.; Spasojević, V. Synthesis, morphology, microstructure and magnetic properties of hematite submicron particles. *J. Alloys Compd.* **2011**, *509*, 7639−7644.
(64) Gajović, A.; Silva, A. M. T.; Segundo, R. A.; Šturm, S.; Jančar, B.; Čeh, M. Tailoring the phase composition and morphology of Bi-doped goethite-hematite nanostructures and their catalytic activity in the degradation of an actual pesticide using a photo-Fenton-like process. *Appl. Catal. B Environ.* **2011**, *103*, 351−361.
(65) Yue, J.; Jiang, X.; Zeng, Q.; Yu, A. Experimental and numerical study of cetyltrimethylammonium bromide (CTAB)-directed synthesis of goethite nanorods. *Solid State Sci.* **2010**, *12*, 1152−1159.
(66) Paige, C. R.; Snodgrass, W.; Nicholson, R. V.; Scharer, J.; He, Q. The effect of phosphate on the transformation of ferrihydrite into crystalline products in alkaline media. *Water, Air, Soil Pollut.* **1997**, *97*, 397−412.
(67) Weatherill, J. S.; Morris, K.; Bots, P.; Stawski, T. M.; Janssen, A.; Abrahamsen, L.; Blackham, R.; Shaw, S. Ferrihydrite formation: the role of Fe13 Keggin clusters. *Environ. Sci. Technol.* **2016**, *50*, 9333.
(68) Sakakibara, M.; Tanaka, M.; Takahashi, Y.; Murakami, T. Redistribution of Zn during transformation of ferrihydrite: effects of initial Zn concentration. *Chem. Geol.* **2019**, *522*, 121−134.
(69) Ford, R. G.; Kemner, K.; Bertsch, P. M. Influence of sorbate-sorbent interactions on the crystallization kinetics of nickel-and lead-ferrihydrite coprecipitates. *Geochim. Cosmochim. Acta* **1999**, *63*, 39−48.

https://dx.doi.org/10.1021/acsearthspacechem.9b00261
ACS Earth Space Chem. 2020, 4, 335−344